AIAA JOURNAL
Vol. 34, No. 10, October 1996

Implicit High-Order Compact Algorithm for Computational Acoustics

K.-Y. Fung*
University of Miami, Coral Gables, Florida 33124-0624
Raymond S. O. Man†
University of Arizona, Tucson, Arizona 85721
and
Sanford Davis‡
NASA Ames Research Center, Moffett Field, California 94035-1000

Accurate solution of the linearized, multidimensional Euler equations for aeroacoustics as a system of simple wave equations is demonstrated. If organized, this system has unambiguous, easily implemented boundary conditions allowing waves of same group speeds to pass through numerical boundaries or comply with wall conditions. Thus, the task of designing a complex multidimensional scheme with approximate boundary conditions reduces to the design of accurate schemes for the simple wave equation. In particular, an implicit compact finite difference scheme and a characteristically exact but numerically *n*th-order-accurate boundary condition are used. This low-dispersion scheme has a third-order spatial accuracy for various types of nonuniform meshes, fourth-order accuracy on uniform meshes, and by choice a temporal accuracy of second order for algorithmic simplicity as the Crank–Nicolson scheme. The robustness and accuracy of the scheme and the validity of the system decoupling are demonstrated through a series of numerical experiments and comparisons with published results, including the recent Institute for Computer Applications in Science and Engineering, NASA Langley Research Center, benchmark problems of acoustic and convective wave propagation in Cartesian and cylindrical domains and reflection at stationary and/or moving boundaries.

Nomenclature

A, B	= coefficient matrices of the Euler equations
a_k, b_k	= coefficients of numerical schemes
c	= wave speed
E, E^{-1}	= forward and backward shift operators, respectively
G	= complex-valued amplification factor
H	= Heaviside function
i	= $\sqrt{-1}$, complex constant
K	= order of interpolants
k	= wave number
L_k	= interpolant associated with the kth node
M_x, M_y	= Mach number components
Ni	= end index of a grid where a wave exits
p	= pressure
r	= ratio between neighboring spacings of a nonuniform grid; after Eq. (3), radial coordinate
t	= time
$\boldsymbol{U}$	= wave vector
$\tilde{\boldsymbol{U}}$	= wave vector in characteristic form
u, v	= wave variables, velocity components in x and y, respectively
x, y	= spatial coordinates
α	= correction factor
δ_x	= difference operator in x
δ_x^2	= $E^{-1} + E - 2$, second difference operator
ε	= numerical damping coefficient
ν	= Courant number
ϕ	= phase angle of G
ω	= wave frequency

Subscripts

A, B	= association with A and B matrices, respectively
a, b	= values at upstream and downstream boundaries, respectively
j, k	= grid indices
m, p	= association with the backward and forward indices, respectively

Superscripts

n	= time level
$()^*$	= most recent value

Presented as Paper CEAS/AIAA 95-010 at the CEAS/AIAA 1st Joint Aeroacoustics Conference, Munich, Germany, June 12–15, 1995; received June 28, 1995; revision received Jan. 31, 1996; accepted for publication Feb. 2, 1996.

*Professor, Department of Mechanical Engineering. Member AIAA.
†Graduate Student; currently Research Associate, Department of Aerospace and Mechanical Engineering.
‡Chief, Fluid Mechanics Laboratory Branch. Associate Fellow AIAA.

I. Introduction

FOR various reasons, direct time-domain solution by finite difference methods, especially of the implicit type, has not been a widely accepted numerical approach to wave propagation problems.[1] Chief among the reasons cited for its unpopularity is the inability of a majority of popular, robust, and successful numerical schemes to track waves with low dispersion and dissipation for large distances.[2] Successful, popular approaches to wave propagation problems, e.g., underwater acoustics, by finite differences do exist but are predominantly indirect, spatial approximations of the so-called parabolic wave equation[3] (Helmholtz) in the frequency domain. Many space–time higher-order explicit schemes have been proposed, e.g., by Tam and Webb.[4] Being explicit and higher order, these schemes inevitably involve multilevel, broadband data structure and algorithmic nonuniformity at domain boundaries. Higher-order schemes with simple data structure, two time levels, and tridiagonal matrices are possible,[5,6] but it is not clear how these schemes can be implemented for solution of practical problems involving more than one spatial dimension without compromising solution accuracy.

Here, a class of high-order schemes for solving the convection (simple wave) equation on nonuniform meshes is derived. A commonality of these schemes is the absence of purely spatial truncation error terms lower than second order. Because of the absence of a

truncation error term proportional to the third spatial derivative of the dependent variable, this class of schemes has low dispersion comparable to the most accurate scheme possible for a three-point two-level stencil on uniform mesh. Among the schemes derived here, the most accurate scheme has fourth-order temporal–spatial accuracy but is not suitable for some systematically stretched grids or extension to systems of conservation laws. A compact spatial fourth-order scheme is possible, but may allow the growth of high-wave-number components on grids with large stretching ratio. Finally, a compact, spatial third-order, low-dispersion scheme with damping for all high-wave-number components and in conservation form, regardless of the stretching ratio, is introduced. The robustness of these schemes is tested and compared on grids with stretching ranges from random to systematic.

These schemes, like all other schemes for simple wave propagation that involve a centered stencil, by themselves without an alternative scheme for the endpoints are incomplete and insufficient to ensure accuracy. Here, a class of higher-order one-sided schemes based on the method of characteristics is derived for the endpoint where waves are propagating out, and is progressively more effective in the reduction of reflections attributable to artificial boundaries, or the size of the domain.

The third-order compact scheme together with an nth-order interpolated end value based on the method of characteristics constitute the building block for construction of solution of wave propagation here.

For problems of more than one spatial dimension, the key issue is whether they can be converted into a system of simple waves for each of which the direction of propagation is known a priori and the corresponding boundary condition is known or enforceable. It is shown through the ICASE/LaRC[7] benchmarking cases that the propagation of aeroacoustic waves, consisting of a combination of acoustic, entropic and vortical waves, is reducible to a system of simple waves. This equivalence implies that algorithms developed for one spatial dimension are immediately applicable for multidimensions, that the computation for each simple wave can be advanced in parallel with that of the others, and that the size of the computational domain can be as small as the region of interest.

II. Low-Dispersion Compact Schemes

In his 1986 review paper, Candel[1] remarked that implicit finite difference schemes had not been reported in acoustic-wave applications, and illustrated the potential savings resulting from their unconditional stability over the Courant–Friedrichs–Lewy-restricted explicit schemes by an application of the Crank–Nicolson scheme to the propagation of acoustic wavelets in a close-end duct. However, it is arguable[2] that because the time-step restriction for solution accuracy is comparable to that for algorithmic stability, the advantage of implicit methods is seen only when the spatial resolution of the spectral contents of the solution is amply sufficient. Clearly, the choice cannot be made on the basis of stability or accuracy alone. Algorithmic simplicity, including implementation of boundary conditions, especially in multidimensional applications is equally, if not more, important. A prime reason for using explicit methods, despite their inefficiency, which nowadays can be compensated by massively parallel computer architecture, is the simplicity in the data structure, if only all boundary conditions are also explicit. Unfortunately, this is not the case in unsteady problems. Pressure, being of prime interest in most cases, is not known a priori and cannot simply be given at the boundary as a function of time. However, aside from having to cope with the difficulty of implementing certain types of boundary condition, implicit methods, as illustrated by Davis[6] using his optimum space–time fourth-order difference scheme, can afford a data structure as simple as three-point two-level and a savings of as much as 60% fewer mesh points per wavelength per dimension than a three-point explicit method. Whereas a comparable explicit method, the dispersion-relation-preserving difference scheme of Tam and Webb[4] for instance, involves a five-point four-level data structure and seven-point one-sided schemes for boundary points. If the ultimate application of these schemes involves other distinct flow features and/or complex boundaries that necessitate the use of nonuniform grids, accuracy, algorithm robustness, data structure simplicity, and solution efficiency all must be considered together for a fair assessment of their effectiveness.

For uniform mesh, weighted differencing has been used on a three-point two-level computational molecule to produce all known finite difference methods,[5] including a temporal second-order spatial fourth-order-accurate compact scheme and the temporal and spatial fourth-order scheme derived and proposed separately by Davis.[6] Here, similar techniques are used to derive schemes suitable for propagation of phase-sensitive waves over nonuniform meshes.

The most general three-point two-level stencil for the convection equation

$$\frac{\partial u}{\partial t} + c\frac{\partial u}{\partial x} = 0 \tag{1}$$

is

$$a_0 u_j^{n+1} + a_1 u_{j-1}^{n+1} + a_2 u_{j+1}^{n+1} = b_0 u_j^n + b_1 u_{j-1}^n + b_2 u_{j+1}^n \tag{2}$$

Here, u_j^n denotes the solution $u(x, t)$ at the spatial node x_j and n times the temporal advancement Δt. The coefficients a_k and b_k, chosen by design, characterize the accuracy, stability and usefulness of a scheme. The choice of a three-point stencil allows the use of a single parameter $r = (\Delta x_{j+1})/(\Delta x_j)$ to characterize grid nonuniformity.

Let a locally plane wave of the form $e^{i\omega t + ikx}$ propagate through a nonuniform mesh of spacing $\Delta x = \Delta x_j = x_j - x_{j-1}$. The amplitudes at two time levels can be related to form the characterizing complex-valued amplification factor

$$G = e^{i\omega\Delta t} = \frac{b_0 + b_1 e^{-ik\Delta x} + b_2 e^{ikr\Delta x}}{a_0 + a_1 e^{-ik\Delta x} + a_2 e^{ikr\Delta x}}$$

If, instead, in Eq. (2) Taylor-series expansion is used to express the values at different points of the stencil, the truncation error can be obtained. For example, the Crank–Nicolson-type (CNT) scheme with centered differencing for the spatial derivative, $(\partial u/\partial x) \approx (\Delta u_j/\Delta x_j)$, has the truncation error

$$\mathrm{TE} = -\frac{c(r-1)\Delta x}{2}u_{xx} - \frac{c^3\Delta t^2}{12}u_{xxx} - \frac{c(r^2 - r + 1)\Delta x^2}{6}u_{xxx} + \mathcal{O}(\Delta x, \Delta t)^3$$

which is formally only first-order accurate when used on a nonuniform grid, i.e., $r \neq 1$.

The compact difference approximant for spatial derivative, $\delta_x u_j$, can be written as

$$(a_m E^{-1} + a + a_p E)\delta_x u_j = \frac{(b_m E^{-1} + b + b_p E)u_j}{\Delta x}$$

where the shift operators are defined as $Eu_j = u_{j+1}$ and $E^{-1}u_j = u_{j-1}$ and the coefficients to be determined are a_m, a, a_p, b_m, b, and b_p. For simplicity, these coefficients are chosen to be functions of r only. Because five of the above coefficients are independent, the spatial gradient, at best, can be approximated to fourth-order accuracy. With trapezoidal integration, the finite difference equivalent of Eq. (1), $\Delta t\delta_t u_j + \nu\Delta x\delta_x u_j = 0$, when put into the form of Eq. (2) will have the coefficients

$$a_0 = 1 + (\nu b/2), \qquad a_1 = a_m + (\nu b_m/2), \qquad a_2 = a_p + (\nu b_p/2)$$

$$b_0 = 1 - (\nu b/2), \qquad b_1 = a_m - (\nu b_m/2), \qquad b_2 = a_p - (\nu b_p/2)$$

where $a = 1$ is set for convenience, and $\nu = c(\Delta t/\Delta x)$ is the Courant number. The maximum spatial accuracy of fourth order is obtained when the coefficients are

$$a_m = \frac{r^2}{(r+1)^2}, \qquad a = 1, \qquad a_p = \frac{1}{(r+1)^2}$$

$$b_m = -\frac{2r^2(r+2)}{(r+1)^3}, \qquad b = \frac{2(r-1)}{r}, \qquad b_p = \frac{2(2r+1)}{r(r+1)^3}$$

This compact fourth-order scheme for nonuniform mesh (C4N) has

$$\mathrm{TE} = -\frac{c^3\Delta t^2}{12}u_{xxx} + \frac{c^3 r(r-1)\Delta x\Delta t^2}{24(r^2+r+1)}u_{xxxx} + \mathcal{O}(\Delta x, \Delta t)^4$$

This scheme reduces to Noye's fourth-order linear finite element (LFE) scheme[5] on a uniform mesh and maintains its accuracy on a nonuniform grid as well. This is because the spatial approximant reduces back to the (2, 2) Padé approximant for three-point two-level differencing for uniform mesh ($r = 1$), with amplification and phase error identical to what has been shown by Beam and Warming[8] for the fourth-order version of their scheme when used with trapezoidal time integration.

As mentioned, C4N has only a second-order temporal accuracy, but there is no pure spatial error term lower than fourth order. However, the second term on the right-hand side above is a third-order cross term involving both Δx and Δt. It can be seen by a comparison of the complex amplification factors that because of the absence of the spatial second-order truncation error term that is proportional to the third derivative of u the improvement in phase over CNT is comparable to that of LFE, whereas the absence of the third-order pure spatial error term ($r = 1$) only brings a very slight reduction of the error in the amplification magnitude. Because the switch to compact differencing introduces two more coefficients—five instead of the original three—and only one is needed to eliminate that second-order term, a free coefficient can be used for the design of a scheme with some other desirable characteristic instead of the marginal improvement of the amplification magnitude. This defines a family of schemes that will be spatially third-order accurate in general.

For instance, by stipulating $b = 0$, the resulting approximant has coefficients

$$a_m = -\frac{r(r-2)}{(r+1)^2}, \qquad a = 1, \qquad a_p = \frac{2r-1}{(r+1)^2}$$

$$b_m = -\frac{6r}{(r+1)^3}, \qquad b = 0, \qquad b_p = \frac{6r}{(r+1)^3}$$

This is a rather simple result that will again reduce back to the Padé approximant for uniform mesh. The scheme, which is called the compact third-order scheme for nonuniform mesh (C3N), has

$$\mathrm{TE} = -\frac{c^3\Delta t^2}{12}u_{xxx} - \frac{c^3(r-1)\Delta x\Delta t^2}{24}u_{xxxx} + \frac{c(r-1)(r+1)^2\Delta x^3}{72}u_{xxxx} + \mathcal{O}(\Delta x, \Delta t)^4$$

For r close to unity, both compact schemes have phase accuracy essentially that of the LFE scheme because the spatially related third-order truncation error terms all have a factor of $(r - 1)$. The major distinction between them is that, at high grid wave numbers $k\Delta x$, the modulus $|G|$ of C4N is greater than unity for a compressing grid $r < 1$ and less than unity for an expanding grid, Fig. 1a, whereas that of C3N, Fig. 1b, is exactly the opposite except for the highest $k\Delta x$ where it is less than unity for both expanding and compressing grids. A wave moving in the direction of an expanding grid becomes less and less resolved because of increasing $k\Delta x$. The unresolved portion often appears as spurious reflections traveling in the opposite direction toward the grid compression. Thus, C4N amplifies the spurious reflections attributable to waves traveling on an expanding grid, and C3N provides a damping. This desirable feature is, in fact, a result of setting $b = 0$.

First, the schemes are tested on a domain with periodic boundary condition to avoid having to address effects of alternative schemes for endpoints and boundary conditions. Following Noye,[5] a Gaussian pulse, i.e., $u(x, 0) = \exp[-100(x - 0.5)^2]$, is placed in the domain, $0 \le x \le 1$, as initial condition. The domain is discretized into 50 points to have a slightly higher resolution, and a smaller time step of 0.008 is used to match the Courant number of 0.4, as in Ref. 5. Four different grids are used. Grid A is a simple uniform grid. The others are nonuniform. Two of them represent the extremes in systematic variation, and the last one is completely lacking in order except the inherent periodicity. Grid B is called a sawtooth grid where the spacing between grid points alternates between wide and narrow, with about 1.1 as r, the ratio of wide-to-narrow spacing. Grid C is called a compressed–expanded grid because points are clustered near the periodic ends and dispersed in the middle. The stretching ratio r varies smoothly from around 1.3 in the expanding region to the reciprocal value of about 0.87 in the compressing region. Grid D is obtained by displacing each grid point of the uniform grid by a random amount less than a quarter of the nominal spacing. Therefore, the absolute minimum spacing possible will be half, whereas maximum will be double. The probability of any amount of displacement is intended to be equal. The solutions after four periods, or 500 time steps, are plotted.

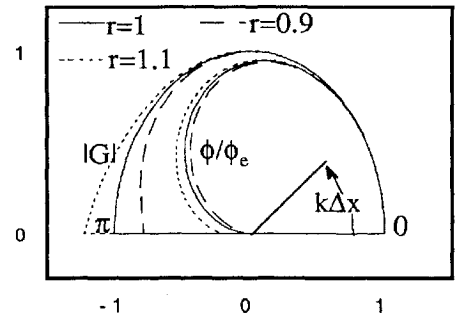

Fig. 1a Modulus $|G|$ and phase ϕ (normalized by the exact ϕ_e) for C4N for different r.

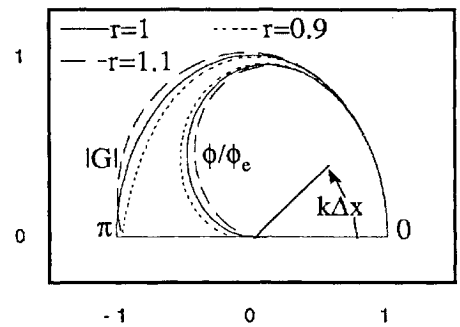

Fig. 1b Modulus and phase for C3N for different r.

Figure 2a almost reproduces a similar figure in Ref. 5, showing that the CNT scheme is highly dispersive and incapable of resolving the Gaussian pulse (dashed line) on the uniform grid as tick-marked on the x axis. Figure 2b shows that, on the sawtooth grid, with cancellation of alternating errors attributable to the sawtooth nonuniformity, the CNT scheme behaves as on a uniform grid. Figure 2c shows that, on the compressed–expanded grid, the CNT scheme behaves much worse, losing completely any phase coordination with the principal pulse, whereas Fig. 2d shows that, on the random grid, phase coordination is the same as on the uniform grid but with embedded wiggles resulting from the randomness.

Of all three-point two-level schemes of Eq. (2) the temporal–spatial fourth-order scheme (TS4) proposed by Noye[5] and independently by Davis[6] gives the optimum and close to exact solution on the uniform mesh for which it was derived and almost as good on the other types except that on the compressed–expanded grid the solution becomes unstable and fails after five time steps. Being identical to each other and equivalent to the LFE scheme[5] on the uniform grid, the compact schemes, C4N and C3N (Figs. 3a–3d), give solutions far better than those of CNT and nearly as good as TS4 on the other grids except for some slight dispersion of high frequency—most noticeably on the compressed–expanded grid, which has lower resolution in the expanding region.

The effort for solving Eq. (2) is the same as that for CNT, one inversion of a tridiagonal matrix for each time step, but a comparable solution using CNT requires a grid roughly eight times finer. In other words, the savings of using compact differencing is eight times less storage and correspondingly eight times faster.

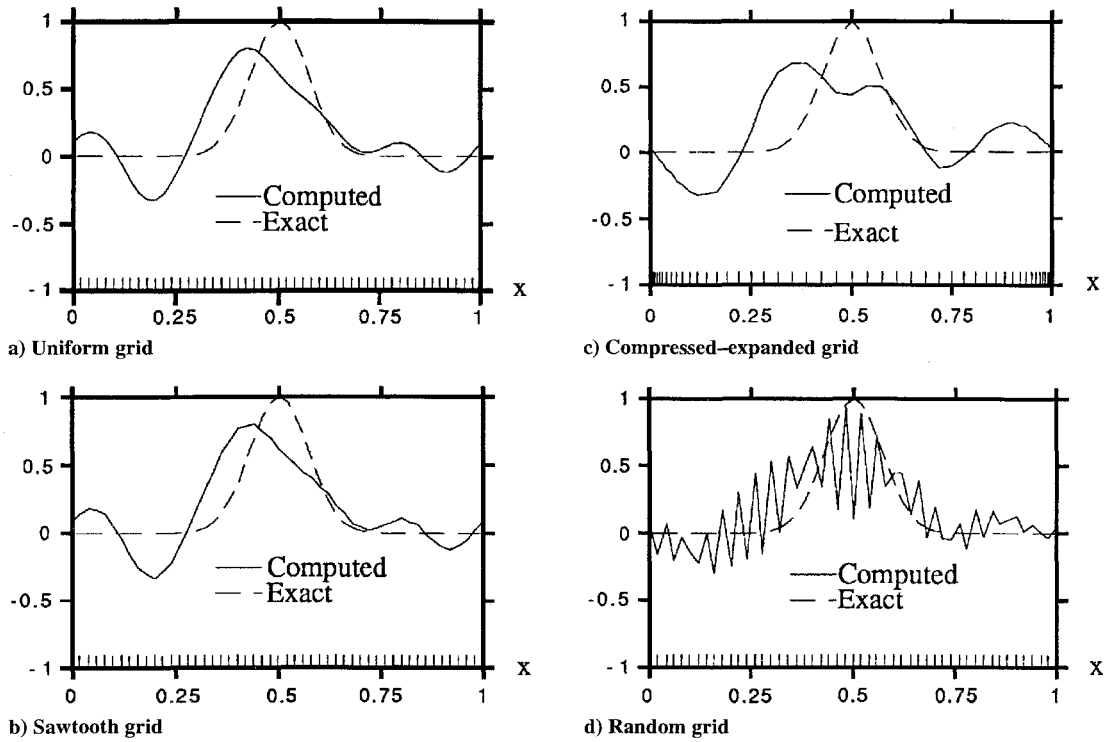

Fig. 2 Computed Gaussian pulses using CNT. Tick marks on the x axis denote grid point distribution.

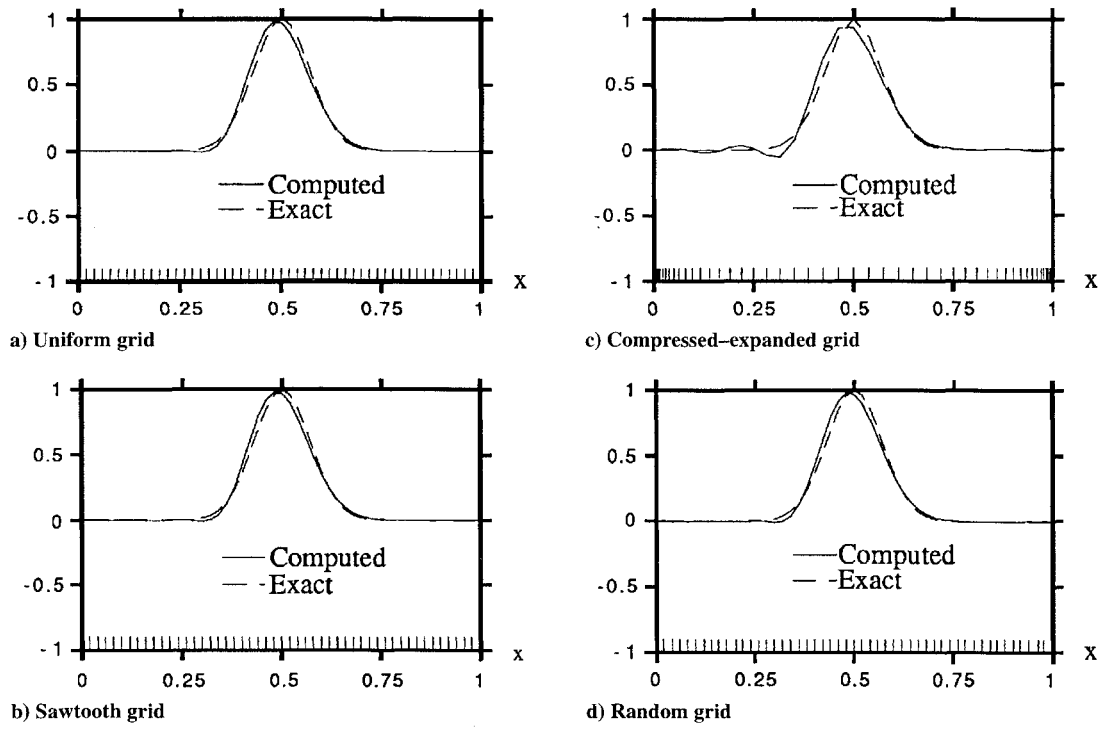

Fig. 3 Computed Gaussian pulses using C3N.

III. Schemes for Endpoints

By itself, Eq. (2) is incomplete for a solution of Eq. (1), which describes the propagation of a wave from point a to point b, left to right, assuming $c > 0$. At the end opposite to the direction of propagation $u(a, t)$ must be specified, whereas at the other end $u(b, t)$ should obey the same equation in theory, but in practice can only follow one-sided schemes. A common remedy is to approximate the spatial derivative using one-sided difference formulas, which pose no implementation difficulty for explicit schemes. For implicit schemes, one-sided formulas for the spatial and temporal derivatives inevitably either complicate the data structure or degrade the scheme to a lower order. They also may cause long-time instability.[9]

Because the schemes considered here are of higher order, the following scheme is proposed to preserve the tridiagonal structure:

$$u_{Ni}^{n+1} = u_c = \begin{cases} \sum_{k=0,K} L_k(x_c) u_{Ni-k}^n; & \nu \le 1 \\ \sum_{k=0,1} L_k(t_c) u_{Ni-1}^{n+1-k}; & \nu > 1 \end{cases} \tag{3}$$

The endpoint Ni, the value u_{Ni}^{n+1} is updated according to the method of characteristics as the value at x_c, depicted in Fig. 4 between points Ni and $Ni - 1$ when $\nu \le 1$, interpolated from $K + 1$ interior values u_{Ni-k}^n using Kth-order interpolants L_k, or at t_c interpolated backward from u_{Ni-1}^n and u_{Ni-1}^{n+1} using a linear interpolant when $\nu > 1$—for it is only necessary that the temporal accuracy of Eq. (3) be, at

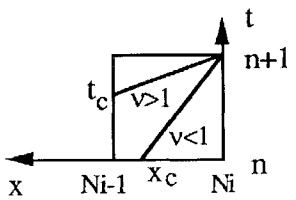

Fig. 4 Boundary scheme.

most, one order less than the scheme[10] that, by choice, is second order. Equation (3) maintains the implicitness and simplicity of a tridiagonal data structure while allowing choices of spatial as well as temporal accuracy of any desirable order. The important distinction between the present scheme and other spatially upwind schemes is that regardless of the number of upwind points, the rule of domain of dependence will be violated by all explicit schemes for large enough ν, so that they are not unconditionally stable. Other implementations of higher-order implicit schemes would inevitably enlarge the system bandwidth without ensuring long-time stability[9] of the system. By a simple switch to backward interpolation in time for $\nu > 1$, the rule of domain of dependence is observed and the overall bandwidth is preserved. For the C3N interior scheme, simple numerical experiments have verified that higher-order interpolants did not improve the temporal accuracy. It has also been demonstrated that this scheme allows the computation of a system of acoustic waves forced at both ends of an acoustic cavity for thousands of wavelengths traveled and bounces between the ends without appreciable phase error and instability.[11]

To test the effectiveness of Eq. (3), a fourth-order Lagrangian interpolant is used for computing the exit of the Gaussian pulse $u(x, t) = 0.5 \exp\{-\ln 2[(x-t)/3]^2\}$ on the domain $20 \geq x \geq -20$ at the right-hand boundary. Unless specified, all solutions presented from here on were computed using the numerically determined optimum time step of $\Delta t = \frac{1}{8}$, further reduction of which led to no significant improvement. This is because of the dispersive nature of the leading temporal truncation error $-[(c^3\Delta t^2)/12]u_{xxx}$ of C3N and C4N. A small value $\Delta t = \frac{1}{8}$ is effective enough to suppress leading numerical dispersion below the spatial truncation error. Figure 5a shows, at $t = 27$, packets of spurious fluctuations of magnitude 5×10^{-4} trailing behind the pulse as its left shoulder is within a few grid points out of the domain. After the pulse has completely left the domain at $t = 40$ (Fig. 5b), the fluctuations congregate at the left-hand boundary, where no wave is allowed to escape, and rebound toward the right-hand boundary, where some reflection is bound to occur because Eq. (3), being one-sided, has dispersion characteristics different from those of a centered scheme. The spurious fluctuations linger on with a slowly reducing magnitude even after long times (Fig. 5c). However, the use of an eighth-order interpolant instead of the same fourth order used in the compact schemes reduces the magnitude of the spurious reflection by a factor of 20 for four more additions and multiplications, which amounts to the work of adding one grid point.

Application of compact differencing to the spherical wave equation having an additional source-like term (category 1, Problem 2, of Ref. 7)

$$\frac{\partial u}{\partial t} + \frac{u}{r} + \frac{\partial u}{\partial r} = 0$$

is achieved by modifying the coefficients of Eq. (2) according to the difference equation:

$$(a_m E^{-1} + a + a_p E)[\delta_t u + (u/r)] + \nu(b_m E^{-1} + b + b_p E)u = 0$$

However, the application of Eq. (3) is simpler if instead of u the variable ur is used, which amounts to replacing L_k by $L_k(r_k/r_0)$. Figure 6a shows the computed wave

$$u(r, t) = (5/r)H(t - r + 5)\sin\omega(t - r + 5)$$

on the domain [5, 450] as the front reaches $r = 400$. The $1/r$ decay is well captured up to the second peak for just a small phase shift at the front. Figure 6b shows the same solution but computed on the truncated domain [5, 45], showing no noticeable reflections from the numerical boundary at $x = 45$ or instability for long-time integration.

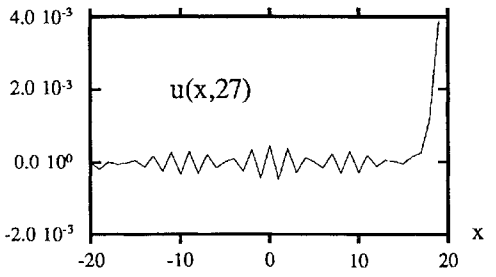

Fig. 5a Spurious fluctuations attributable to fourth-order boundary conditions.

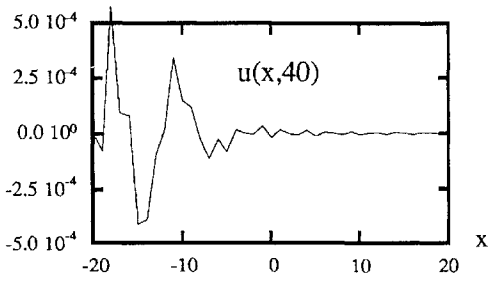

Fig. 5b Congregation of dispersed reflections.

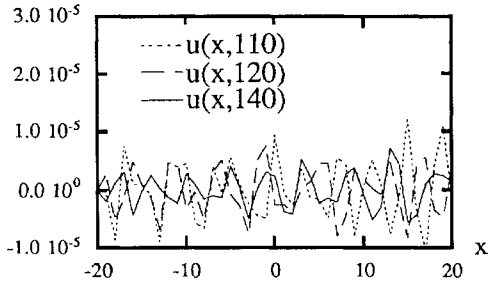

Fig. 5c Trapped dispersion residues.

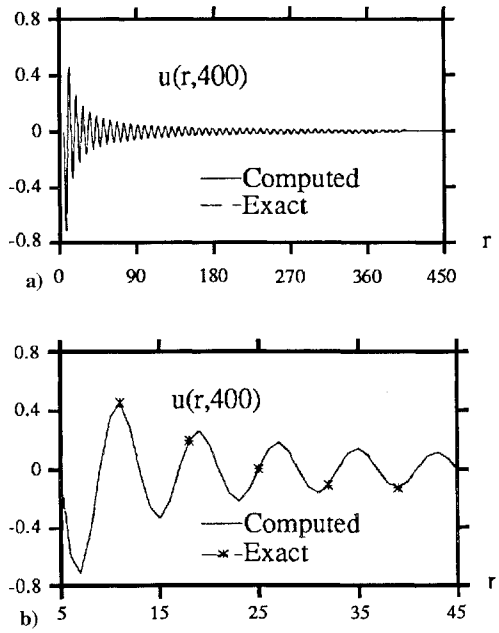

Fig. 6 Application of C3N a) to spherical wave $u(r,t) = H(5 + t - r)\sin\omega(5 + t - r)/r$, ($\omega = \pi/4$, $\Delta t = 0.125$) and b) with fourth-order boundary conditions imposed at $r = 45$.

IV. Multidimensional Extensions

One drawback in the application of implicit schemes to multidimensional problems is the drastic increase in system bandwidth for each additional dimension unless operator splitting or approximate factorization is used. However, a factorized or split scheme often involves intermediate variables that have no clear connection to the physical variables on which certain constraints are to be satisfied. Hence, the success of an implicit scheme for multidimensional problems hinges on whether the dependent variable in each factorized or split step can be consistently related to the physical constraints at boundary. This seems to be the case for aeroacoustic problems governed by the linearized Euler equations in Cartesian coordinates:

$$\frac{\partial U}{\partial t}+\frac{\partial AU}{\partial x}+\frac{\partial BU}{\partial y}=0$$

where

$$U=\begin{bmatrix}\rho\\ u\\ v\\ p\end{bmatrix},\qquad A=\begin{bmatrix}M_x,1,0,0\\ 0,M_x,0,1\\ 0,0,M_x,0\\ 0,1,0,M_x\end{bmatrix},\qquad B=\begin{bmatrix}M_y,0,1,0\\ 0,M_y,0,0\\ 0,0,M_y,1\\ 0,0,1,M_y\end{bmatrix} \tag{4}$$

Equation (4) can be split into two sets of equations:

$$\begin{cases}\delta_t U+\delta_x AU=0\\ \delta_t U+\delta_y BU=0\end{cases}$$

which then can be transformed into two sets of first-order decoupled equations

$$\begin{cases}\delta_t \bar{U}_A+\delta_x \Lambda_A \bar{U}_A=0\\ \delta_t \bar{U}_B+\delta_y \Lambda_B \bar{U}_B=0\end{cases}$$

corresponding to the characteristic variables

$$\bar{U}_A=\begin{bmatrix}\rho-p\\ v\\ u-p\\ u+p\end{bmatrix},\qquad \bar{U}_B=\begin{bmatrix}\rho-p\\ v-p\\ u\\ v+p\end{bmatrix}$$

and eigenvalues

$$\Lambda_A=\begin{bmatrix}M_x,0,0,0\\ 0,M_x,0,0\\ 0,0,M_x-1,0\\ 0,0,0,M_x+1\end{bmatrix},\qquad \Lambda_B=\begin{bmatrix}M_y,0,0,0\\ 0,M_y-1,0,0\\ 0,0,M_y,0\\ 0,0,0,M_y+1\end{bmatrix}$$

Subscripts A and B correspond to the coefficient matrices A and B, which define the transformation from the physical variables to the characteristic variables, or the corresponding processes of wave propagation for each spatial dimension. It is clear that the last three equations in both transformed sets can be solved independently of the first, that only p affects ρ, and thus the first equation is needed only to find ρ after knowing p. The first equations in transformed sets A and B describe the convection of entropy $\rho-p$ in two distinct directions at corresponding speeds M_x, M_y. Being linear and independent, these equations, or processes, can be advanced in any order. The second equation in set A describes the convection of a vortical disturbance v at the speed M_x, whereas the third and fourth equations describe the propagation of acoustic disturbances at the receding speed M_x-1 and advancing speed M_x+1. The advancements of v and u in set A follow two distinct processes, and hence are independent, whereas the roles of u and v exactly reverse in set B. Thus the linearized Euler equations (4), which describe the convection of entropy and vorticity and the propagation of acoustic pulses, can be seen as eight one-dimensional modes of wave propagation at speeds corresponding to their eigenvalues. Unlike factorization, which approximates the governing equation for easy inversion, splitting simply acknowledges the decomposition of vectors and the possibility of advancing their components separately. The two sets are indeed coupled through the common scalar variable p, which adjusts to the vortical and acoustical disturbances from all directions, and through which mass conservation is ensured.

It should be emphasized that, in general, the vector components and their governing equations in curvilinear coordinates cannot be decoupled into systems of directionally independent equations. In his construction of nonreflecting boundary conditions based on the linearized two-dimensional Euler equations in Cartesian coordinates for explicit schemes, Gill,[12] in Sec. II, proposed approximations of various degrees of accuracy to accommodate the coupling between gradients tangential and normal to a wave-exiting boundary to satisfy well-posedness. Similarly, in their implementation of Moretti's λ-scheme for fast solution of the steady Euler equations for transonic airfoils, Dadone and Moretti[13] employed Beaming–Warming type directional splitting to reduce the system bandwidth. The temporal inaccuracies in these approaches are a result of ineffective directional decouplings.

Once split, the system becomes a set of one-dimensional wave equations, which can be solved using the compact schemes, or any appropriate schemes. A problem is set by specifying a value for each wave mode at the incoming end. Take, for example, the set A variables

$$\bar{U}_A=\begin{bmatrix}\rho_a-p_a\\ v_a\\ u_b-p_b\\ u_a+p_a\end{bmatrix}$$

which correspond to the eigenvalue matrix

$$\Lambda_A=\begin{bmatrix}M_x,0,0,0\\ 0,M_x,0,0\\ 0,0,M_x-1,0\\ 0,0,0,M_x+1\end{bmatrix}$$

and assume that $0<M_x<1$. All variables corresponding to right running characteristics must be specified at the left boundary $x=a$ except the third specified at the right $x=b$. For an undisturbed upstream or downstream, these values are unambiguously given. However, as disturbances propagate outward beyond b, the information for the third variable, which should come from the value at a location beyond b, is lost. Depending on the type of disturbance and approximation used, different degrees of reflection are found in the solutions as they are presented and discussed later.

Unlike other approaches[7,12] that employ local approximations to inhibit, suppress, or force the domain-entering components at numerical boundaries to comply with the desired conditions, the directionally decoupled systems here require specification of the domain-entering components while allowing the outgoing components to exit freely because of the effectiveness of Eq. (3). Thus, setting the domain-entering components at finite boundaries to zero corresponds to an exact enforcement of the outgoing-only (nonreflective) boundary conditions for any domain, regardless of size. For a wall, the wall-bound characteristic variable, e.g., $v-p$, is solved first; then the domain-entering component $v+p$ is set to comply with any condition on v, e.g., $v+p=-(v-p)$ to enforce $v=0$. This ordering establishes a causality relation between the acoustic components, which should be solved one after the other as two arrays or combined into a large array with the wave-exiting end of one array connected to the wave-entering end of the other to satisfy the constraints on both ends. The joint array has a cyclic boundary condition that can be solved using standard cyclic tridiagonal solvers.

V. Multidimensional Test Problems

For testing algorithmic symmetry, the pressure, vortical and entropic Gaussian pulses of Ref. 7 (category III problems; see also Ref. 4) respectively initiated at the center and two-thirds to the downstream boundary on the horizontal axis of symmetry were computed on the unity-spacing 201×201 grid. The field is swept in an alternating $x-y-y-x$ fashion with a time-step unit of $\frac{1}{8}$ and a convecting Mach number of 0.5. Figure 7a shows the density

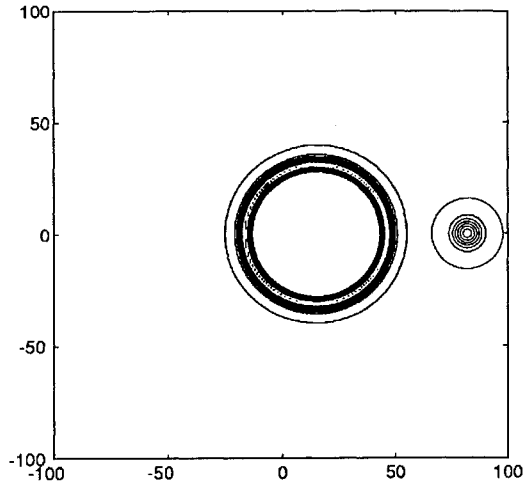

Fig. 7a Horizontally convected acoustic and vortical pulses at $t = 30$ (contour levels: 0.00 + increments of 0.015).

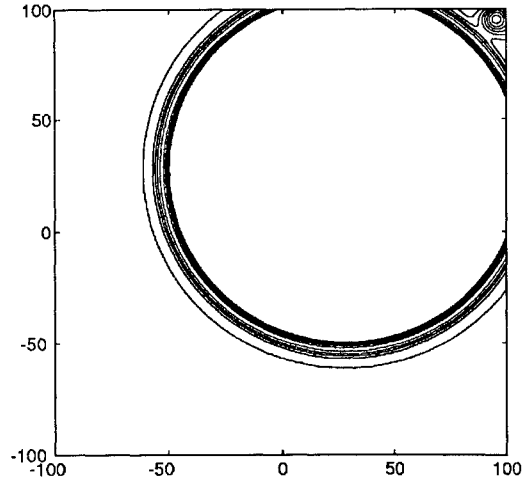

Fig. 7b Diagonally convected acoustic and vortical pulses at $t = 80$ (contour levels: 0.00 + increments of 0.015).

contours of the vortical pulse and the expanding acoustic pulse after being convected horizontally 15 grid points downstream from their initial positions. Perfect numerical symmetry is found in both pulses before their fronts reach the downstream boundary, confirming the validity of the present directional-splitting approach and the one-dimensional nature of linear wave propagation in Cartesian coordinates. As the wave front of the acoustic pulse catches up with the vortical pulse at the downstream boundary, a slight asymmetry is observed in the density contours around the exiting vortex resulting from the boundary condition. These pulses were then initiated and convected along the diagonal of the grid. Again, perfect symmetry is found until the vortical pulse exits the domain at the upper-right corner, Fig. 7b, where slight contour distortion attributable to the boundary condition is discernible.

At an exit plane the receding characteristic variable $(u - p)$ is undisturbed (i.e., equal to zero or $u = p$) until the arrival of a wave resulting from convection. If the solution domain was not truncated, this receding part of the exiting waves, for which u and p are not necessarily equal, would re-enter the exit plane. The common practice of setting $u - p|_b = 0$, referred to as BC0, could cause a phase shift and, correspondingly, reflections along the domain-entering characteristics. Much weaker reflections are found when $u - p$ is kept at the current value $|^*$ from the sweep in the alternate direction, referred to here as BC1, viz., $(u - p)^{n+1} = u - p|^*$. Figure 8 shows the pressure contours at $t = 20$ of the impingement of an acoustic pulse (category 4, Problem 1, of Ref. 7) on the horizontal wall with the wall condition, $v = 0$. Figure 9a shows the fronts of

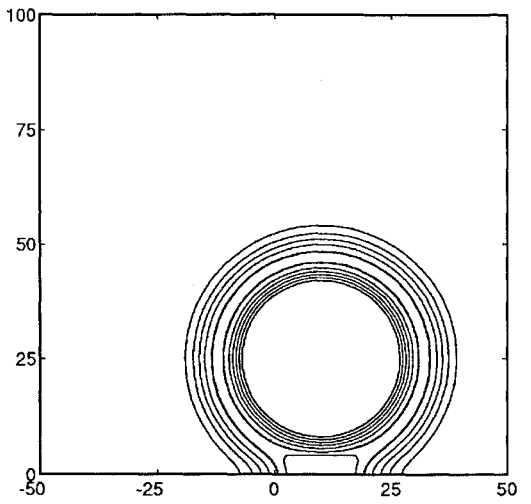

Fig. 8 Impingement and reflection of an acoustic pulse at $t = 20$ on the horizontal wall (contour levels: 0.00 + increments of 0.03).

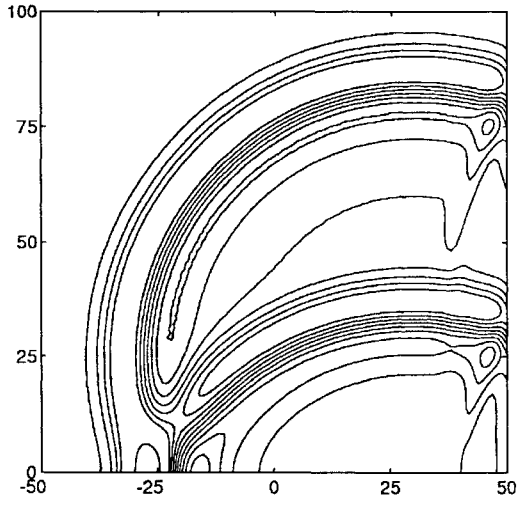

Fig. 9a Spikes of reflection at numerical boundary attributable to BC0 (contour levels: −0.11 + increments of 0.02).

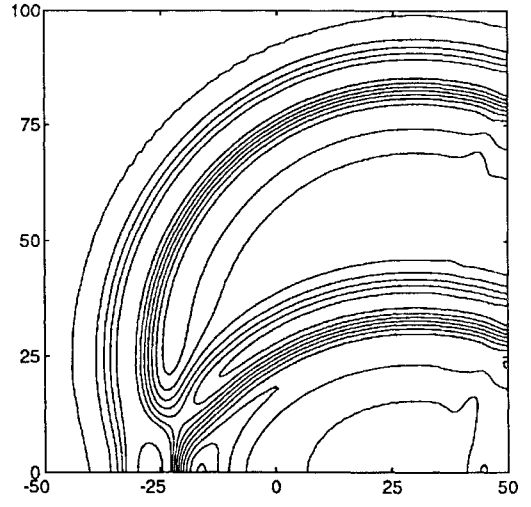

Fig. 9b Weak reflections at numerical boundary attributable to BC1 (contour levels: −0.10 + increments of 0.02).

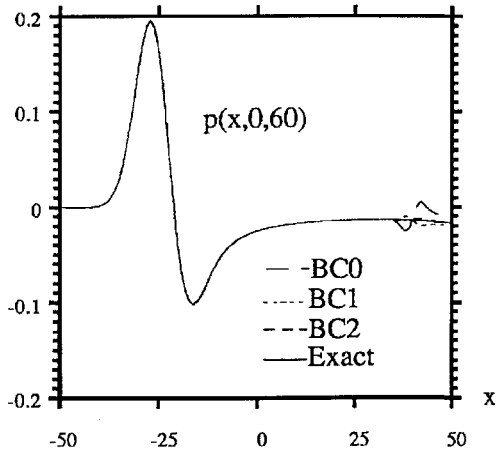

Fig. 10 Comparison of wall pressure distributions showing exact enforcement of wall boundary condition and the effect of various exit conditions at $x = 50$.

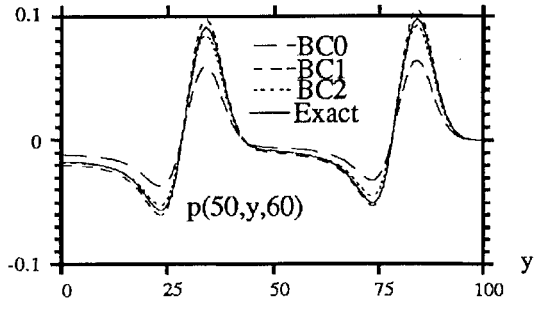

Fig. 11 Comparison of pressure distributions computed by applying various exit conditions at the downstream numerical boundary $x = 50$.

the partially bounced and expanding pulse and spikes of reflections resulting from the application of applying BC0 at the downstream boundary ($x = 50$) of the ($-50 < x < 50$; $0 < y < 100$) computational domain. Much weaker reflections are found when BC1 is used (Fig. 9b). While the condition of impingement is exactly enforced as clearly shown by the comparison in Fig. 10 of wall pressure with the exact values, the computed pressure distribution at the domain boundary at $x = 50$ corresponds to roughly 20% reflections for applying BC0 but less than 10% even at the peaks for BC1 according to the comparison in Fig. 11. The amounts of reflection corresponding to different exit conditions are also evident in the labeled wall pressure distributions in Fig. 10.

The present method allows all interior waves to leave the domain boundary cleanly because of the effectiveness of Eq. (3). All conditions at domain boundaries correspond to specification of the domain-entering components. In the absence of convection ($M_x, M_y = 0$), there will be no domain re-entering waves and thus no reflections. BC1 simply corresponds to the same way all interior values are computed. Whereas for $M_x > 1$, all conditions are given at the upstream boundary and thus the solution is incapable of having reflections at the downstream boundary. Indeed, the case shown here with $M_x = 0.5$ represents the worst reflections at the downstream boundary of all Mach numbers. Furthermore, the proportional amount of reflections does not change with the size of the computational domain, which can be as small as the domain of interest, and that further improvement, shown as BC2 in Figs. 10 and 11, can be made by applying an ad hoc correction factor α in $(u-p)^{n+1} = (1+\alpha)(u-p)^* - \alpha(u-p)^n$ to account for the loss of information attributable to domain and, hence, solution truncation. Nevertheless, unless specified, all results herein were computed with BC1 enforced at all exit boundaries.

The authors have not investigated the use of asymptotic outgoing-only expressions[4] for exit condition, which may be domain and problem dependent and inadequate for domain re-entering waves as well.

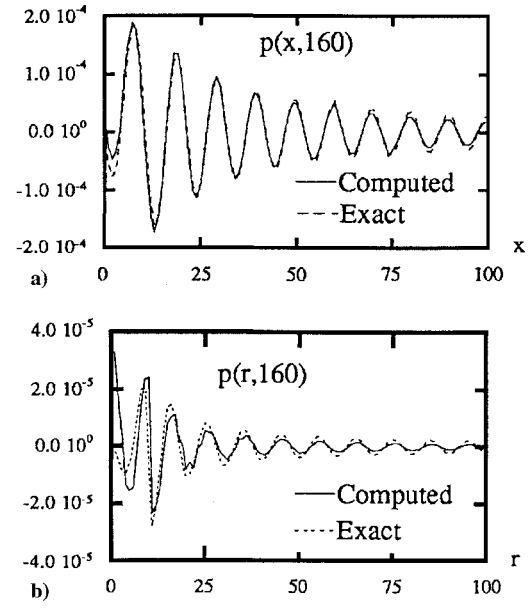

Fig. 12 Comparsion of computed pressure variations: a) axial and b) radial.

The extension to problems in cylindrical coordinates, is nontrivial in that unlike in Cartesian coordinates, the acoustic part of the split equations in the radial direction cannot be transformed into uncoupled characteristic components because of the source-like term v/r, viz.,

$$\delta_t \begin{bmatrix} u_1 \\ u_2 \\ u_3 \\ u_4 \end{bmatrix} + \delta_r \begin{bmatrix} 0,0,0,0 \\ 0,0,0,0 \\ 0,0,-1,0 \\ 0,0,0,1 \end{bmatrix} \begin{bmatrix} u_1 \\ u_2 \\ u_3 \\ u_4 \end{bmatrix} + \begin{bmatrix} 0 \\ 0 \\ \dfrac{-(u_3+u_4)}{2r} \\ \dfrac{u_3+u_4}{2r} \end{bmatrix} = 0$$

However, the coupling between the acoustic components is weak, and the source-like term can be treated explicitly to a second order in time to maintain the same simplicity in data structure as in Cartesian coordinates, e.g.,

$$u_3^{n+1} = u_3^n + (\Delta t/2)\delta_r\left(u_3^{n+1} + u_3^n\right) + (\Delta t/2r)\left[u_4^n + u_3^n + (\Delta t/2)\delta_r\left(u_4^n - u_3^n\right)\right]$$

Another complication arises because of the transformation singularity at the radial symmetry point $r = 0$. Numerically, this is just a boundary point where the incoming characteristic variable $v - p$ turns into the outgoing variable $v + p$ to satisfy the condition at $r = 0$, where v also vanishes, but not necessarily v/r. Fortunately, the assumption that v/r is regular and, hence, approaches the adjacent value at $r = \Delta r$ proved adequate for the computation of the acoustic field of a harmonically moving piston (category 4, Problem 2, of Ref. 7). Figure 12 gives a comparison of pressure variations with the exact pressure along and normal to the piston axis at $t = 160$. In particular, the agreement in phase is excellent, but the computing time for 1280 time steps of four variables over 101×101 grid points is 49 s on a SGI-Indy, or 11% of that for evaluating the analytical expression for $p(x, r, 160)$ for the same field points using the C double precision intrinsic Bessel functions and a 40th-order Gaussian quadrature. Because there is no convection or re-entering of receding waves in this case, all waves, physical or spurious, are allowed to propagate out at the numerical boundaries $x = 100$ and $r = 100$, and no noticeable changes were found in the solution as the cycles repeat for much longer times or computed on smaller domains.

For uniform grids, the compact schemes presented are nondissipative but dispersive for short waves whose presence is unavoidable whenever a discontinuity is involved in the boundary condition. In the case of a piston, for example, the edge of a piston at $r = R$ is a source of discontinuity where the axial velocity changes abruptly from the piston velocity to zero wall velocity. Spurious waves immediately disperse unless they are either filtered or damped. Here, a damping, $\varepsilon = 0.01$, consistent with a three-point scheme and proportional to the second derivative

$$\varepsilon \frac{\Delta t}{\Delta x^2} \delta_x^2 \frac{u_j^{n+1} + u_j^n}{2}$$

is found adequate for the present applications.

VI. Conclusions

The effectiveness of C3N closed with a class of outgoing boundary conditions for various types of grids and aeroacoustic problems has been established. This implicit compact scheme, though not the most accurate one on a uniform grid, is simple to implement, robust under all conditions tested, and requires standard tridiagonal solvers and negligible storage overhead to invert.

The equivalence between the propagation of acoustic waves in two spatial dimensions and that of a system of one-dimensional simple waves in Cartesian coordinates is shown. The characteristic variables in each spatial dimension can be decoupled and ordered according to their one-dimensional propagation process. The extension of this decoupling to three spatial dimensions in Cartesian coordinates is straightforward. All solutions presented, regardless of the number of spatial dimensions, have been obtained by passing segments of self-contained, one-dimensional arrays through standard solvers, which may concurrently occupy a massive array of computers for rapid data processing.

Contrary to others, the present approach requires specification of the domain-entering components at domain boundaries. These components should correspond to the local physical conditions to ensure no spurious reflections. It is shown here how the spurious reflections are reduced but not completely eliminated, for which further research is warranted.

Acknowledgment

Partial support for Raymond Man under NASA Grant NCA 2-707 is gratefully acknowledged.

References

[1]Candel, S., "A Review of Numerical Methods in Acoustic Wave Propagation," *Recent Advances in Aeroacoustics*, edited by A. Krothapalli and C. A. Smith, Springer–Verlag, New York, 1986, pp. 339–410.

[2]Roe, P., "Technical Prospects for Computational Aeroacoustics," DGLR/AIAA Paper 92-02-032, May 1992.

[3]Lee, D., Botseas, G., and Papadakis, J. S., "Finite Difference Solutions to the Parabolic Wave Equation," *Journal of the Acoustical Society of America*, Vol. 70, No. 3, 1981, pp. 795–800.

[4]Tam, C. K. W., and Webb, J. C., "Dispersion-Relation-Preserving Difference Schemes for Computational Acoustics," *Journal of Computational Physics*, Vol. 107, No. 2, 1993, 262–281.

[5]Noye, J., "Three-Point, Two-Level Finite Difference Methods for the One-Dimensional Advection Equation," *Computational Techniques and Applications*, CTAC-85, edited by J. Noye and R. May, North-Holland, Amsterdam, 1986, pp. 159–192.

[6]Davis, S., "Low-Dispersion Finite Difference Methods for Acoustic Waves in a Pipe," *Journal of the Acoustical Society of America*, Vol. 90, No. 5, 1991, pp. 2775–2781.

[7]Tam, C. K. W., "Benchmark Problems and Solution," ICASE/LaRC Workshop on Benchmark Problems in Computational Aeroacoustics (Hampton, VA), Oct. 1994, pp. 1–13.

[8]Beam, R. M., and Warming, R. F., "An Implicit Finite-Difference Algorithm for Hyperbolic Systems in Conservation-Law Form," *Journal of Computational Physics*, Vol. 22, 1976, pp. 87–110.

[9]Carpenter, M. H., Gottlieb, D., and Abarbanel, S., "Time-Stable Boundary Conditions for Finite-Difference Schemes Solving Hyperbolic Systems: Methodology and Application to High-Order Compact Schemes," *Journal of Computational Physics*, Vol. 111, No. 2, 1994, pp. 220–236.

[10]Gustafsson, B., "The Convergence Rate for Difference Approximations to Mixed Initial Boundary Value Problems," *Mathematics of Computation*, Vol. 29, 1975, pp. 396–406.

[11]Tallapragada, B. P., and Fung, K.-Y., "Application of Compact Finite Difference Schemes to One-Dimensional System of Waves," *Proceedings of III ASME GSTC* (Tampa, FL), American Society for Testing and Materials 1995.

[12]Gill, M. B., "Nonreflecting Boundary Condition for Euler Equation Calculation," *AIAA Journal*, Vol. 28, No. 12, 1990, pp. 2050–2058.

[13]Dadone, A., and Moretti, G., "Fast Euler Solver for Transonic Airfoils, Part I: Theory," *AIAA Journal*, Vol. 26, No. 4, 1988, pp. 409–416.